Analysis of Self-Pulsating Sources Based on Regenerative SPM: Ignition, Pulse Characteristics and Stability

Thibault North and Martin Rochette

***Abstract*—We provide design guidelines and resulting outputs of a self-pulsating source based on regenerative self-phase modulation and offset band-pass filtering. We assess the conditions for self-pulsation and discuss the output pulse properties under the influence of spectral separation between the filters and their bandwidth. We also examine the source behavior when the central wavelength of the bandpass filters are subject to increasing spectral separation in the pulse-buffering regime. The results emphasize the role of chromatic dispersion for the reduction of amplitude and timing jitter.**

***Index Terms*—Laser resonator, nonlinear optics, optical pulse regeneration, self-phase modulation (SPM), self-pulsating source.**

I. Introduction

SELF-Pulsating (SP) sources based on cascaded regeneration are a new alternative to conventional mode-locked sources mainly based on saturable absorption. Designs of mode-locked sources include additive pulse mode-locking or semiconductor saturable absorbers [1], [2], defining a fixed phase relationship between the propagating modes. Sources based on cascaded regeneration, however, do not allow a phase-locked laser oscillation, but rather converge toward the propagation of a so-called "eigenpulse", which undergoes periodic changes in its profile and spectrum and is regenerated after every cavity round-trip [3]. Regenerative sources have three main operation regimes. In the degenerate case, the source outputs a continuous wave (CW) signal. Otherwise, the source spontaneously generates pulses from noise in a SP regime, or sustain existing pulses in the pulse-buffering (PB) regime. Unlike conventional mode-locked sources, regenerative sources support the propagation of ultrashort pulses even in cavities as large as ~2 km, they are insensitive to polarization and can sustain one or more pulses in their cavity. Incidentally, the architecture of regenerative sources directly enables nonlinear pulse compression at its output from the self-phase modulation (SPM) broadened pulse spectrum [4]. Furthermore, it was shown in [4] that the experimental behavior of this cavity configuration was well predicted by numerical models.

Manuscript received July 10, 2013; revised September 18, 2013 and October 11, 2013; accepted October 11, 2013. Date of publication October 17, 2013; date of current version November 8, 2013. This work was supported by the National Optics Institute, Quebec city, QC, Canada.

The authors are with the Department of Electrical and Computer Engineering, McGill University, Montreal, QC, H3A 2A7, Canada (e-mail: thibault.north@mail.mcgill.ca; martin.rochette@mcgill.ca).

Color versions of one or more of the figures in this paper are available online at http://ieeexplore.ieee.org.

Digital Object Identifier 10.1109/JLT.2013.2286331

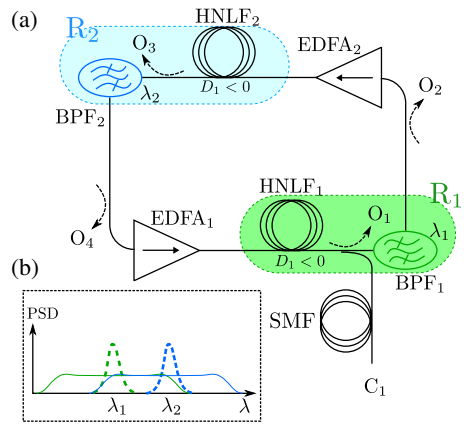

Fig. 1. Source setup: (a) paired regenerators in closed loop and (b) SPM broadening and offset filtering.

Optimization rules for 2R regenerators were reported previously [5]–[9], and a theoretical study of cascaded 2R regenerators was performed by Pitois *et al*. [10], [11]. In the latter references, the authors describe the evolution of noise and pulses that are input to cascaded regenerators with controlled amounts of chromatic dispersion, nonlinearity and filter offset. In contrast with the regenerator cascade of [10], a SP source based on cascaded regenerators takes advantage of the saturable nature of the amplifiers in order to determine the dynamics of pulse propagation.

In this paper, we investigate the ignition conditions of SP sources in the SP regime for filter spectral bandwidth between 0.1 and 4 nm and adequate filter offsets. We also describe the source operation in PB regime, and show the importance of chromatic dispersion to ensure stability. Finally, the output pulse properties are discussed. In contrast with previous references, we include higher order nonlinear effects and third-order dispersion (TOD), which significantly alters the source behavior by inducing an asymmetry on the pulse spectrum.

This paper is organized as follows: first, the source architecture is presented along with its numerical model. Second, the conditions for self-starting are discussed. Finally, we describe the pulse properties and the source stability in specific configurations.

II. Source Architecture and Setup

The numerical model used in this paper is based on experimental values reported in [4]. Fig. 1(a) illustrates paired regenerators in a closed loop, composed of two highly nonlinear

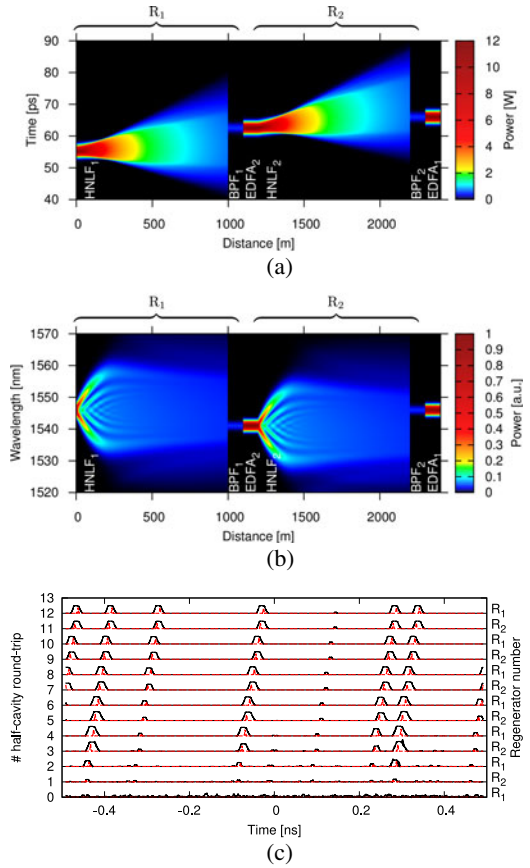

Fig. 2. (a) and (b) Maps of the pulse propagation, in the time and frequency domains, in steady-state. The length of the amplifying and filtering regions is increased for readability. (c) Self-starting from noise. Signal power after the HNLF (solid line) and after filtering (red dashed line). (a) Time domain. (b) Spectral domain. (c) Self-starting from ASE.

fibers (HNLFs) with normal dispersion, two tunable band-pass filters (BPFs), and two erbium-doped fiber amplifiers (EDFAs). For simplicity, the modeled setup is symmetrical and both HNLFs have the same parameters: a constant waveguide nonlinear coefficient $\gamma = 12.5\ \mathrm{W^{-1}km^{-1}}$, a variable chromatic dispersion coefficient D in $\mathrm{ps\ nm^{-1}km^{-1}}$, a fixed dispersion slope $S = 0.0074\ \mathrm{ps\ nm^{-2}km^{-1}}$ a fixed loss $\alpha = 1.86\ \mathrm{dB\ km^{-1}}$ and a fixed length $L = 1007$ m. The EDFAs are characterized by an unstaturated gain G_0 and a saturation power P_{sat}. The band-pass filters $\mathrm{BPF_1}$ and $\mathrm{BPF_2}$ are spectrally centered at $\lambda_{1,2}$ with a full width at half maximum (FWHM) bandwidth $\Omega_{1,2}$. The spectral offset between $\mathrm{BPF_1}$ and $\mathrm{BPF_2}$ is $\Delta = |\lambda_1 - \lambda_2|$. Fig. 1(b) depicts the main spectral features of the source at their operation wavelengths λ_1 and λ_2. Pulses propagating in $\mathrm{HNLF_1}$ at λ_2 undergo spectral broadening by the conjugated effects of SPM and dispersion. After filtering at $\mathrm{BPF_1}$ and reamplification a similar spectral broadening is experienced by pulses in $\mathrm{HNLF_2}$, and finally $\mathrm{BPF_2}$ reestablished λ_2 as the central wavelength for the next cavity round-trip. In Fig. 2(a) and (b), the temporal and spectral power profile of an eigenpulse is shown as a function of the propagation distance. During propagation in the HNLF, the pulse broadens in the first 300 m and then acquires a pedestal. Its final FWHM duration is $10\times$ higher than its initial duration. Spectrally, oscillations due to SPM build up in the first 200 m. The conjugated effects of SPM and dispersion then flatten the central part of the spectrum, and transfer energy toward its edges. Fig. 2(c) presents the process of pulse generation from ASE.

The source is observed at outputs O_{1-4}, and after nonlinear recompression at C_1.

III. Numerical Model

Pulse propagation in the cavity is simulated using a software developed within our group, and inspired by [12]. Propagation through all segments of fiber is described by the nonlinear Schrödinger equation,

$$\frac{\partial A}{\partial z} + \frac{\alpha A}{2} + \frac{i}{2}\beta_2\frac{\partial^2 A}{\partial T^2} - \frac{1}{6}\beta_3\frac{\partial^3 A}{\partial T^3} = i\gamma\left(|A|^2 A + \frac{i}{\omega_0}\frac{\partial}{\partial T}(|A|^2 A) - T_R A\frac{\partial |A|^2}{\partial T}\right) \quad (1)$$

taking into account the effects of chromatic dispersion of the second (β_2) and third (β_3) orders, the nonlinearity (γ), the medium attenuation (α), self-steepening and the Raman effect ($T_R = 3$ fs). Also in equation (1), A is the electric field, T the time, ω_0 the carrier frequency, and $i = \sqrt{-1}$.

Equation (1) is solved numerically using the fourth order Runge-Kutta in the interaction picture method with an adaptive step size [13], [14], on an Nvidia GeForce GTX 550Ti using Reikna [15] on top of PyOpenCL [16], with 2^{15} sample points in time and frequency, for a large temporal window and a good temporal and spectral resolution. Amplifiers are characterized by a saturable output power P_{out} modeled following [17]

$$P_{\mathrm{out}} = P_{\mathrm{in}} G_0 \exp\left[-\frac{P_{\mathrm{out}} - P_{\mathrm{in}}}{P_{\mathrm{sat}}}\right] \quad (2)$$

where P_{out} is related to the input power P_{in} with the small signal gain G_0 and the saturation power P_{sat}. When explicitly specified, the amplifier noise is included in the calculations [18]. A single polarization component is considered to interfere with the oscillating signal, the other component being orthogonal. The total ASE power is

$$P_{\mathrm{ASE}} = \int_{-\infty}^{\infty} n_{\mathrm{sp}} h\nu_0 (G-1) H_{\mathrm{A}}(\nu - \nu_0)\mathrm{d}\nu \quad (3)$$

where $n_{\mathrm{sp}} = 2$ is the spontaneous-emission factor, h the Planck constant, G is the gain, ν_0 is the central frequency, and H_{A} is the gain profile approximated by a tapered cosine window in the range 1525–1560 nm [19]. BPFs are modeled with a Gaussian profile. Loss is neglected in all components, except for the HNLFs.

The source self-starts from spontaneous emission. A minimum of 20 cavity round-trips are performed for each simulation to assess whether self-starting occurs or not. When self-starting occurs, a steady-state is usually reached within the first 15 cavity round-trips. The setup of Fig. 1 is observed at outputs O_{1-4}, and a time-domain filter is added at outputs O_2 and O_1, providing two additional outputs. These filters are super-Gaussians of order 10, and are centered over the most powerful pulse

with a temporal duration of 3× the pulse FWHM. The Fourier transformed signal therefore shows a profile cleared of the beats induced by the presence of multiple pulses, and spectral features can be measured more accurately.

IV. Results

In Section IV-A, the operation of the SP source of Fig. 1 is observed under a set of different configurations. We assess its ability to self-start from ASE under several values of gain, spectral offset Δ, and filter bandwidth Ω. In Section IV-B, one BPF is spectrally shifted once the source has reached a SP state. In this process, the output pulse properties are investigated and the source stability is analyzed in terms of time and amplitude jitter in Section IV-C.

A. Self-Starting Conditions: Contribution of the Filter Offset

The experimental values of Sun *et al*. [4] are being used for the following simulations: at $\lambda_0 = 1550$ nm, $D = -0.69$ ps nm^{-1}km^{-1} ($\beta_2 = 0.88$ ps^{2}km^{-1}), $S = 0.0074$ ps nm^{-2}km^{-1} ($\beta_3 = 0.012$ ps^{3}km^{-1}), $\alpha = 1.86$ dB. The saturation power, however, is reduced to 6 dBm to limit the number of pulses in the cavity, to avoid overlaps and therefore facilitate the extraction of pulses from the temporal signal.

There are three regimes of operation for a SP source, depending on the filter spacing Δ, as pointed out in [4]. Increasing the value from $\Delta = 0$, the emission transforms from a CW regime, to a SP regime, to a PB regime. In the latter, only existing pulses are sustained, and the source cannot ignite pulses from ASE noise for example when the doped fibers are pumped with increasing power. To assist the realization of such sources, it is necessary to describe the conditions for self-starting, their relationship to the filter offset, the filter spectral bandwidth and the available amplifier gain. Numerical simulations show that the transition between the CW and the SP regimes with increasing Δ occurs gradually. Gaussian pulses build up in the cavity in the first 20 cavity round-trips, but also coexist with CW components, forming a noisy pulsed signal in time, with a noise amplitude that decreases with increasing Δ.

Experimentally, the wavelength dependent attenuation introduced by the cavity components leads to a co-propagating amplified ASE signal. Fig. 3(a) shows the coexistence of these signals in the time domain, with an amplitude jitter of $\sim$4% in power, and Fig. 3(b) depicts the corresponding spectrum. An appropriate time-domain filtering confirms that the pulses profiles in time are associated with the sidelobes of the spectrum, under the influence of SPM, while the noisy signal in time stands spectrally at the intersection of the BPFs.

In a first series of simulations, the operating regimes which allow self-starting are shown as a function of the amplifier gain and the filter spectral offset, from an initial invariant ASE spectrum. In Fig. 4, the normalized filter offset $F = \Delta/\Omega$ is considered, and the source is in a pure pulsing regime with a clear background when $F \gtrsim 1.7$.

Fig. 4 shows the number of oscillating pulses, as well as the ratio of noise over signal power, for several filter bandwidths.

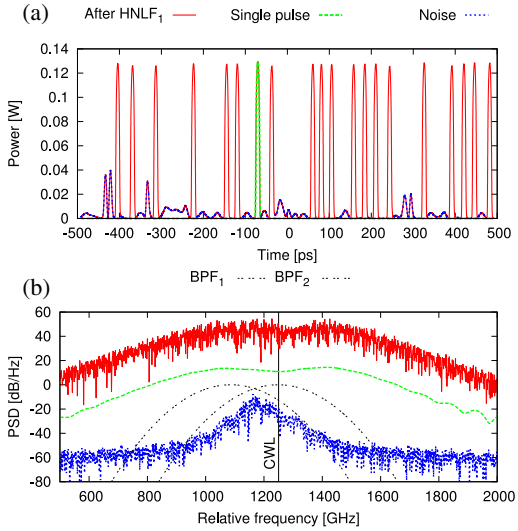

Fig. 3. In (a) noisy signal including a series of eigenpulses (red), and isolated eigenpulse (green) and a noise floor (blue) in the time domain. In (b) spectra of the noisy signal (red), isolated eigenpulse (green), and noise floor (blue). The transmission profiles of BPF_1 and BPF_2, separated by 162 GHz, are also provided.

Self-starting at large Δ is also enabled by an increased gain, but the number of propagating pulses saturates due to the fixed $P_{\mathrm{sat}} = 6$ dBm. It may be noted that for a bandwidth $\Omega = 0.9$ nm and $G_0 = \sim 100$, the operation region spreads from 1.6 to 2.2 nm, which corresponds well with the behavior observed experimentally, in Fig. 4 of [4]. The leftmost gradient of Fig. 4(aa)–(ff) indicates the decrease of noise as Δ increases, and the yellow rightmost region signals the absence of pulses in the cavity.

In [4], self-pulsing operation is demonstrated with filters of bandwidth of 0.4 and 0.9 nm, but this bandwidth can be increased safely at least up to 4.0 nm and more without preventing self-pulsation. For this particular nonlinear medium, a wide range of filter bandwidths leads to self-pulsation. The two conditions for generation of eigenpulses are 1) an adequate spectral separation Δ between the BPF that does at the same time favor pulses over CW oscillation and tolerate an initial ASE propagation, 2) an amplifier gain which is sufficient to trigger SPM broadening from the ASE. Qualitatively, in the case of pulses that are temporally long, for a small filter bandwidth Ω, requirement 2) may be difficult to attain. At large filter bandwidths, the spectral content is more likely to produce a fast varying intensity profile, whose slope induces important amounts of spectral broadening by SPM. In this case, the amplifier gain must be sufficient to sustain pulses of that power spectral density in spite of other cavity losses.

B. Transition in Between the Self-Pulsating and Pulse-Buffering Regimes

Practically, tuning one BPF toward the PB regime is interesting. High values of the normalized filter offset improve the signal over noise ratio, and diminishes the number of pulses in the cavity. Their peak power is therefore increased, and ultrashort pulses can be generated by nonlinear compression at

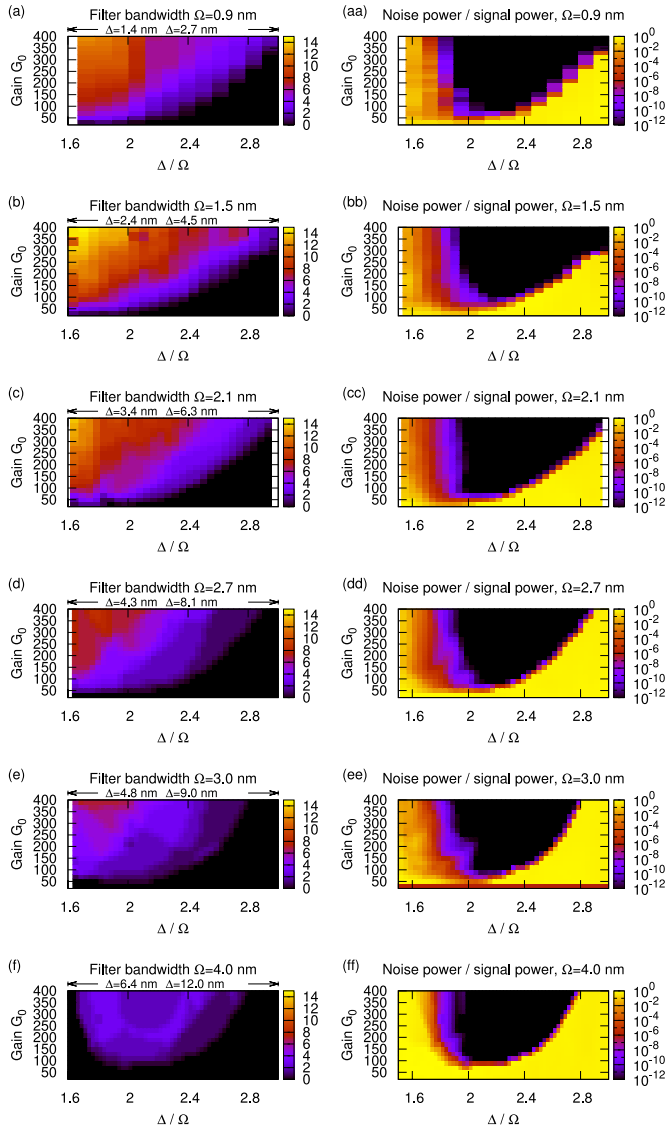

Fig. 4. Left: Number of pulses as a function of the gain and the filter offset Δ, for filter bandwidths of 0.9 to 4.0 nm. Right: corresponding plot of noise/signal power.

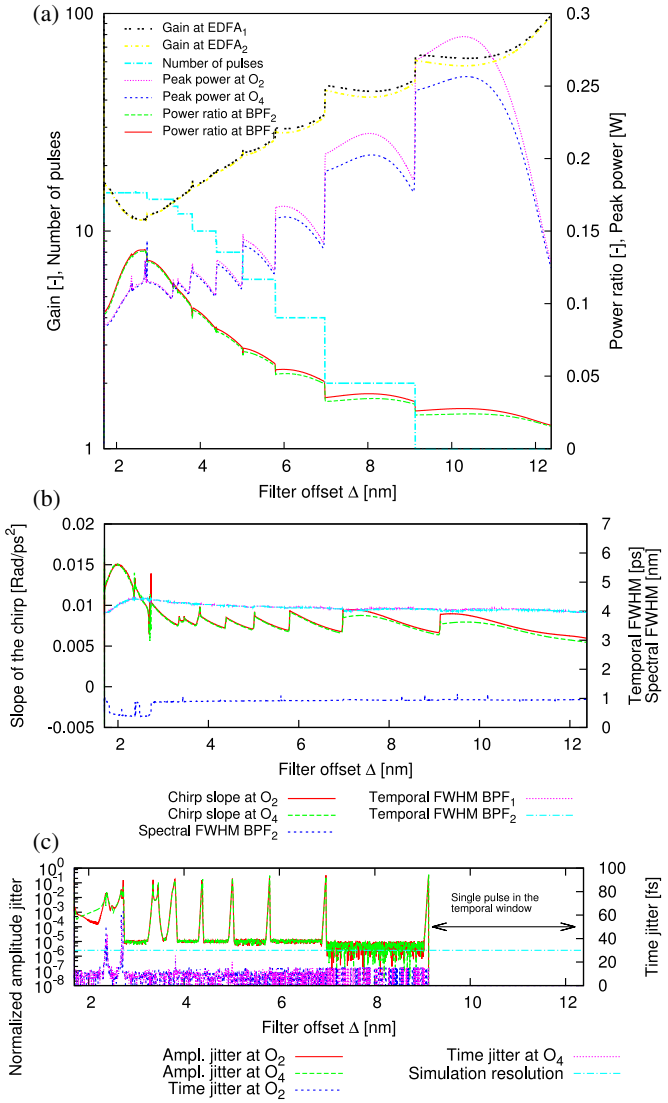

Fig. 5. Transmission at $BPF_{1,2}$, number of pulses and peak power observed in the simulation for $G_0 = 200$. The asymmetry of the SPM-induced spectral broadening due to TOD is responsible for the transmission mismatch between BPF_1 and BPF_2. (b) Chirp slope and pulse temporal width as a function of the filter distance Δ. (c) Amplitude and time jitter after the BPFs.

C_1. In this series of simulations, the source is started from ASE noise with a spectral offset of $\Delta = 1.7$ nm, in SP regime, and spawns 14 pulses in the simulation's temporal window. The BPFs have a spectral FWHM of 0.9 nm, and the unsaturated gain $G_0 = 200$, with $P_{\text{sat}} = 9$ dBm. In order to attain the PB regime, BPF_2 must be spectrally shifted toward longer wavelengths. To ensure a smooth transition, letting the circulating pulses unaffected, the filter is shifted by 5 pm at each consecutive cavity round-trip. Because the time window of 1 ns used in simulations is much shorter than the round-trip period of the source of ~ 10 µs, the number of pulses that circulate in the cavity is limited by the sampling window. Sharp transitions occur when the number of pulse changes, as the available power is redistributed among the remaining ones. Experimentally, however, one can expect to observe a smoother behavior, since $\sim 10^4\times$ more pulses can coexist in the cavity, when the cavity size is ~ 2 km. In Fig. 5, the source is started from ASE and 14 pulses circulate in the simulation's temporal window. After 15 cavity round-trips, filter BPF_2 is shifted at a rate of 5 pm/round-trip. Fig. 5(a) depicts the efficiency of the source, the number of pulses in the cavity, the EDFA gain, and the peak power of circulating pulses as a function of the spectral separation of the BPFs. A maximum of $\sim 13.5\%$ of transmission is reached at a filter offset of 2.6 nm. This corresponds to the position of the first SPM lobe for a nonlinear phase-shift of $\sim 2\pi$ [20]. The discrepancy in gain and pulse peak power, particularly visible at high Δ, indicates that the source tends to lose its unique eigenpulse in favor of two different ones, one per HNLF. Although pulses are of similar FWHM, the TOD of the HNLFs induces an asymmetry on their spectrum [21]. With fibers featuring a positive dispersion slope, the blue-most filter BPF_1 enables a higher transmission than BPF_2, which yields to pulses that are up to 12% more powerful compared to the ones out of BPF_2. In Fig. 5(b), the output chirp

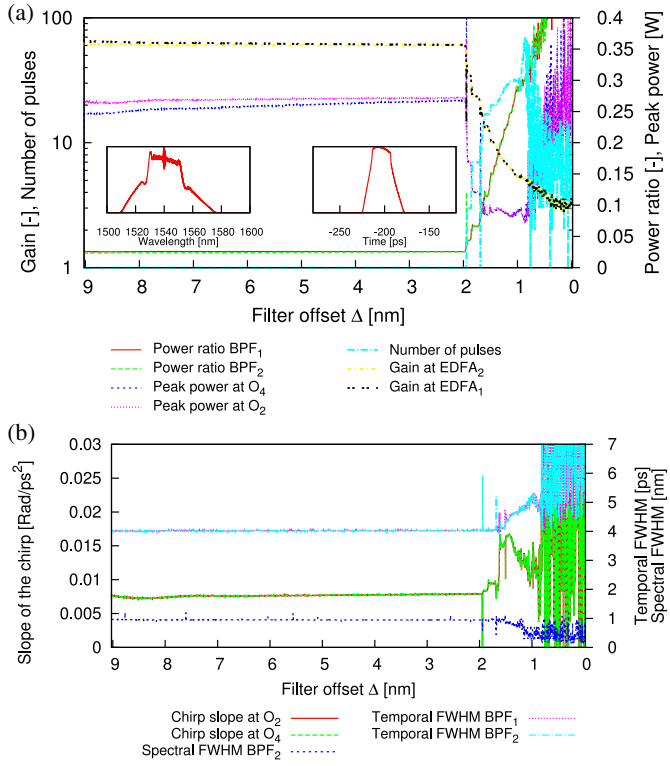

Fig. 6. (a) Transmission at $\mathrm{BPF}_{1,2}$, gain, number of pulses and peak power observed in the simulation for $G_0 = 200$, as the offset Δ is decreased. Insets: typical spectral and temporal shape over the range 9–2 nm. (b) Corresponding chirp slopes and temporal pulse width.

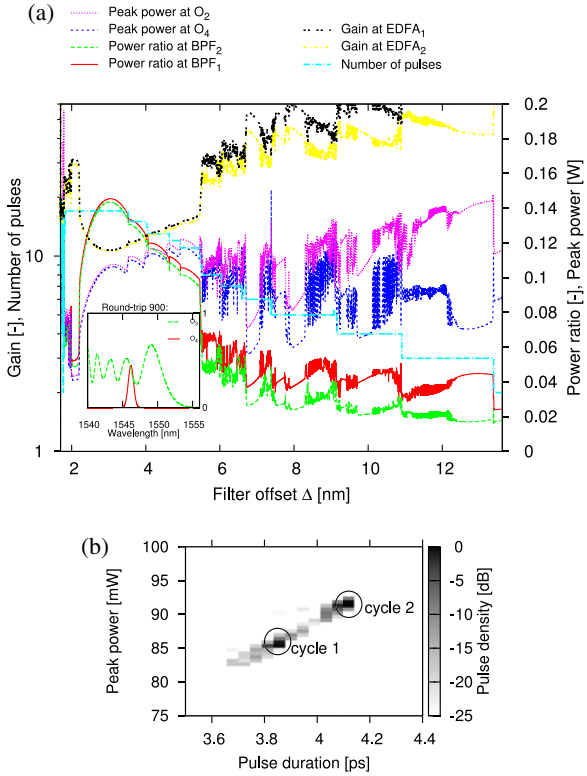

Fig. 7. (a) Peak power, power ratio, gain and number of pulses in the cavity for $G_0 = 200$, $D = -0.173$ ps/nm/km. Inset: For round-trip #900, spectrum at O_3 and O_4. (b) Limit cycles for $D = 0.395$ ps/nm/km and $G_0 = 200$.

slope and pulse FWHM, the pulse temporal FWHM, and the bandwidth at BPF_2 are depicted as a function of the filter offset. Because the chirp is close to linear, the chirp slope refers to the value of the chirp derivative at the position of maximal peak power. In this particular configuration and in setups including a narrow BPF such as this one, the chirp remains low for all Δ, and the pulse has a time-bandwidth product of 0.45. Aside from the discrepancy in peak power, the outputs O_2 and O_4 are interchangeable. In Fig. 5(c), the time and amplitude jitter are depicted as a function of the filter offset. The amplitude jitter is defined as $\delta P/P_0$, where δP is the standard deviation of the peak power of all pulses visible in the temporal window, and P_0 the median peak power. The time jitter measures the pulse-to-pulse time difference between the current and the previous cavity round-trip. The amplitude jitter increases significantly when a pulse is about to be discarded. Temporally, it is observed that most pulses are unequally affected in this process, and undergo a reduction of their peak power. The nonlinear power transfer function of cascaded regenerators quickly discards pulses of low peak power, and a new stable state occurs. At all time, the timing jitter is stable and negligible in the cavity, which is expected for a cascade of 2R regenerators. In Fig. 6, from the configuration depicted in Fig. 5, the spectral offset Δ is decreased once a stable single pulse operation is attained. The amplifiers are modeled with spontaneous emission from equation (3). The single pulse propagating in the cavity is sustained, and the source can not spawn new pulses from ASE when there is no filter overlap, since the 2R regenerator intrinsically rejects ASE noise. It is only when Δ approaches 1.96 nm that new pulses are generated, marking the transition between the PB regime and the SP regimes. In this process, simulations indicate that the amplifier noise is the predominant factor for the generation of new pulses in the cavity, rather than pulse-splitting, which occurs because of the spectral overlap of the BPFs. The wavelength of transition between the SP and PB regimes is hence different whether Δ is increased or decreased.

C. *Stability: Timing and Amplitude Jitter*

As indicated by Fig. 6(a) and (b), the source shows an excellent stability over a wide wavelength range. Once in PB regime, little chirp or peak power variation occur as Δ is altered. This stability originates from the amount of chromatic dispersion accumulated in the HNLFs, which prevents large spectral fluctuation induced by SPM alone. This amplitude jitter is associated with the presence of multiple eigenpulses in the cavity, as reported in [10]. When pulses of different peak power co-propagate, their group-velocity, associated with the effective refractive index and therefore related to their peak power, induces timing jitter and pulse collision. In comparison, Fig. 7(a) features a HNLF with a dispersion $D = -0.173$ ps $\mathrm{nm}^{-1}\mathrm{km}^{-1}$. Numerous instability domains result from the insufficient amount of chromatic dispersion in the nonlinear medium, for filter offset Δ larger than 5.5 nm. By observing the inset of Fig. 7(a), it is apparent that BPF_2 intercepts the SPM-induced spectrum at a position where

the slope of the spectrum is large. In this case, for a fixed filter position, small amplitude variation at the input are translated into large peak power variations at the output and the source experiences an amplitude and a timing jitter. This unstable state is not necessarily permanent, since a pulse is occasionally discarded by pulse collision, and hence resets the source to a stable operation. Fig. 7(b), depicts the coexistence of different eigenpulses in the source, in accordance with [10]. After self-starting, the temporal simulation window contains 23 pulses. Collisions occur in that process, and the number of pulses drops to 21 after 5000 cavity round trips. Since these eigenpulses have different group velocities, collisions occur and ultimately only a single type of eigenpulse is sustained at the steady-state. In regenerative sources, reaching optical wave-breaking is desirable, because this phenomenon flatten the central part of the spectrum, as illustrated in the inset of Fig. 6(a). A large ratio of the dispersive and nonlinear lengths $L_D = T_0^2/|\beta_2|$ over $L_{\mathrm{NL}} = 1/(\gamma P_0)$, ensures that wave-breaking is reached. In addition to that, the input pulse sent to the HNLFs is always chirped, which accentuates this effect. The loss in the HNLFs is also beneficial in terms of stability, because it decreases the importance of nonlinearities while leaving the accumulated dispersion unaffected.

D. Pulse Properties in the PB Regime

Previous work of Sun *et al.* [4] reveals that the chirp of output pulses after filtering increases with the filter bandwidth. The reason behind this observation is that pulses that undergo SPM in a medium of normal dispersion acquire a chirp which is close to linear, and corresponds in the spectral domain to a linear delay function across the broadened spectrum. A broader filter therefore captures spectral components that have a larger relative delay, leading to an increased chirp. In the configuration (f) of Fig. 4 with a gain $G_0 = 100$, it is assessed that the pulses could be recompressed down to 930 fs by the addition of single-mode fiber (SMF) at the output O_2, in good agreement with [4]. This value is close (within 5%) to the value of 880 fs expected for transform-limited pulses, confirming that the chirp is close to being linear. With a BPF bandwidth of 6 nm, the chirp becomes nonlinear due the growing influence of the asymmetries in the SPM-broadened spectrum. Along with the effects of TOD, nonlinear recompression at C_1 therefore saturates at 210 fs for $\Omega = 4$ nm and 6 nm despite the large available bandwidth exceeding 20 nm. Nevertheless, the source shows an excellent stability at large BPF bandwidths, as well as a good efficiency above 20% caused by a large amount of power captured at the filtering stage.

It must also be pointed out that the FWHM of the filtered spectrum depends directly on the shape of the broadened signal. After a filter that faces a dip in the SPM-broadened spectrum, the output pulses can be up to 20% shorter in time than those for which the filter faces a local maximum. Fig. 8(a) illustrates this in the spectral domain, while Fig. 8(b) shows the corresponding time-domain pulses, centered at the origin for simplicity. After a linear shift of BPF_2 toward longer wavelengths in the PB regime, the distribution of temporal FWHM of the pulses emanating from this displacement is presented in Fig. 9, when $P_{\mathrm{sat}} =$ 9 dBm. The pulse width reported in this figure is the median value of the FWHM of pulses visible in the time window, their variance being negligible. Fig. 9(c) and (d) present a larger dispersion of pulse widths due to the instabilities encountered while altering the value of Δ. From that spectral position, if BPF_2 is shifted toward shorter wavelengths, the number of pulses in the cavity remains fixed, at its minimum value. If wavebreaking is reached due to an increased pulse peak power, the spectrum flattens as observed in the inset of Fig. 6, and the distribution of temporal pulse duration will show no dispersion.

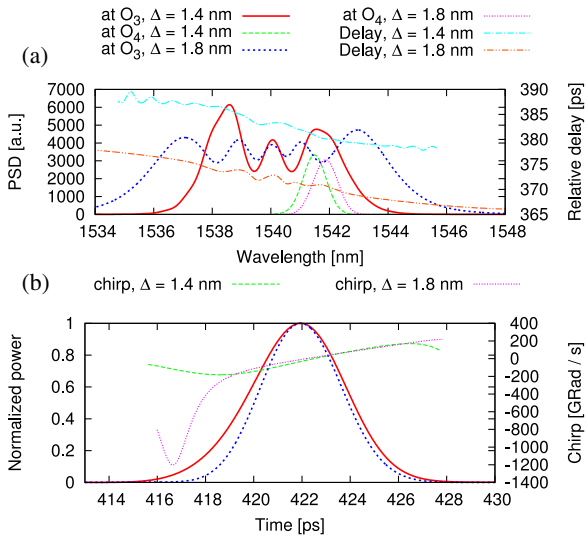

Fig. 8. Spectral and temporal profiles associated to $\Delta = 1.4$ and 1.8 nm for $G_0 = 100$. Different positionnings of the BPFs with respect to the SPM-induced spectrum result into different pulse duration and spectral width.

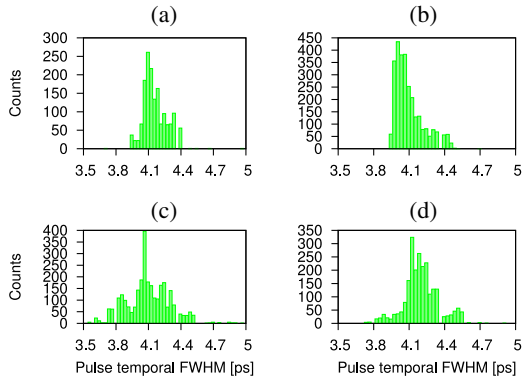

Fig. 9. Temporal FWHM distribution of pulse in PB operation for (a) $G_0 = 100$, (b) $G_0 = 200$, (c) $G_0 = 200$ and a chromatic dispersion $D = -0.173$ ps/nm/km, (d) $G_0 = 200$ and $D = -0.069$ ps/nm/km.

V. Discussion and Conclusion

A numerical study of SP sources based on cascaded regeneration was performed for a set of cavity configurations. Self-starting is observed for a broad range of filter bandwidths, gain values, and filter offsets. The ability of these sources to self-start depends on the gain of the amplifiers being used, while the number of pulses is determined by the saturation power of the amplifiers. Self-starting occurs with an unsaturated gain

that decreases with increasing filter spectral width. As well, the source enters the SP regime with filter bandwidths in the range 0.1 nm–4.0 nm, making this architecture very interesting in practice. The continuously changing temporal profile eigenpulses propagating in the cavity reminds of other types of SP sources such as self-similar or stretched-pulse lasers. In these lasers, linearly chirped pulses are propagating in the cavity, enabling high energies without impairments due to the excess of nonlinearities inside the cavity. The regenerative sources architecture offer such advantages as well, and limitations induced by excessive nonlinearities occur only in the PB regime, when the cavity contains few pulses. By design, regenerative sources however reject a relatively large fraction of their spectrum at the filtering stages, and this is the main obstacle to the generation of pulses of high energies. The TOD of the HNLFs introduces asymmetries in the spectral features of output pulses, as shown in [21], which translate into output pulses of different energies after each regeneration stage. The gain of the EDFAs can be adjusted relatively to the sign of β_3 in order to compensate for this discrepancy.

Pulse properties have also been investigated, and variations in the pulse duration occur in PB regime as the spectral filter offset is altered. The pulse bandwidth is influenced by the shape of the SPM-broadened spectrum after the HNLFs. Especially for large filters, it turns out that the pulse duration can vary by $\sim$20% mainly for this fact. It could be tempting to increase the filter bandwidth in order to generate ultrashort pulses. However, an additional chirp limits the expected pulse shortening. The addition of a standard SMF leads to near transform-limited pulses after the BPFs, and simulations show that subpicosecond pulses can be obtained without nonlinear compression at output $O_{2,4}$. However, nonlinear recompression is bound to the effects of TOD and to the limited spectral broadening that pulses undergo in the nonlinear medium. Finally, amplitude and timing jitters are observed in fibers that have large ratios of dispersive length over nonlinear lengths. This must be kept in mind for the conception of such sources that offer a high nonlinearity and for which the nonlinear length is much smaller than the dispersion length. Such sources are more likely to be unstable if operated with BPFs of relatively narrow spectral widths.

REFERENCES

[1] E. P. Ippen, H. A. Haus, and L. Y. Liu, "Additive pulse mode locking," *J. Opt. Soc. Amer. B*, vol. 6, pp. 1736–1745, 1989.

[2] U. Keller, K. Weingarten, F. Kartner, D. Kopf, B. Braun, I. Jung, R. Fluck, C. Honninger, N. Matuschek, and J. A. der Au, "Semiconductor saturable absorber mirrors (SESAM's) for femtosecond to nanosecond pulse generation in solid-state lasers," *IEEE J. Sel. Topics Quantum Electron.*, vol. 2, no. 3, pp. 435–453, 1996.

[3] M. Rochette, L. R. Chen, K. Sun, and J. Hernandez-Cordero, "Multiwavelength and tunable self-pulsating fiber cavity based on regenerative SPM spectral broadening and filtering," *IEEE Photon. Technol. Lett.*, vol. 20, no. 17, pp. 1497–1499, 2008.

[4] K. Sun, M. Rochette, and L. R. Chen, "Output characterization of a self-pulsating and aperiodic optical fiber source based on cascaded regeneration," *Opt. Exp.*, vol. 17, pp. 10419–10432, 2009.

[5] P. Baveja, D. Maywar, and G. Agrawal, "Optimization of all-optical 2R regenerators operating at 40 Gb/s: Role of dispersion," *J. Lightw. Technol.*, vol. 27, no. 17, pp. 3831–3836, 2009.

[6] L. A. Provost, C. Finot, P. Petropoulos, K. Mukasa, and D. J. Richardson, "Design scaling rules for 2R-optical self-phase modulation-based regenerators," *Opt. Exp.*, vol. 15, pp. 5100–5113, 2007.

[7] M. Rochette, L. Fu, V. Ta"eed, D. Moss, and B. Eggleton, "2R optical regeneration: An all-optical solution for BER improvement," *IEEE J. Sel. Topics Quantum Electron.*, vol. 12, no. 4, pp. 736–744, 2006.

[8] A. Striegler and B. Schmauss, "Analysis and optimization of SPM-based 2R signal regeneration at 40 gb/s," *J. Lightw. Technol.*, vol. 24, no. 7, pp. 2835–2843, 2006.

[9] T.-H. Her, G. Raybon, and C. Headley, "Optimization of pulse regeneration at 40 Gb/s based on spectral filtering of self-phase modulation in fiber," *IEEE Photon. Technol. Lett.*, vol. 16, no. 1, pp. 200–202, 2004.

[10] S. Pitois, C. Finot, L. Provost, and D. Richardson, "Generation of localized pulses from incoherent wave in optical fiber lines made of concatenated Mamyshev regenerators," *JOSA B*, vol. 25, pp. 1537–1547, 2008.

[11] S. Pitois, C. Finot, and L. Provost, "Asymptotic properties of incoherent waves propagating in an all-optical regenerators line," *Opt. Lett.*, vol. 32, pp. 3263–3265, 2007.

[12] A. A. Amorim, M. V. Tognetti, P. Oliveira, J. L. Silva, L. M. Bernardo, F. X. Kärtner, and H. M. Crespo, "Sub-two-cycle pulses by soliton self-compression in highly nonlinear photonic crystal fibers," *Opt. Lett.*, vol. 34, pp. 3851–3853, 2009.

[13] J. Hult, "A fourth-order Runge–Kutta in the interaction picture method for simulating supercontinuum generation in optical fibers," *J. Lightw. Technol.*, vol. 25, no. 12, pp. 3770–3775, 2007.

[14] A. Heidt, "Efficient adaptive step size method for the simulation of supercontinuum generation in optical fibers," *J. Lightw. Technol.*, vol. 27, no. 18, pp. 3984–3991, 2009.

[15] B. Opanchuk, "Reikna, the pure Python GPGPU library," hosted at http://reikna.publicfields.net/

[16] A. Klöckner, N. Pinto, Y. Lee, B. Catanzaro, P. Ivanov, and A. Fasih, "PyCUDA and PyOpenCL: A scripting-based approach to GPU run-time code generation," *Parallel Comput.*, vol. 38, pp. 157–174, 2012.

[17] A. Siegman, *Lasers*. Herndon, VA, USA: Univ. Science Books, 1986.

[18] G. Agrawal, *Lightwave Technology: Telecommunication Systems*. New York, NY, USA: Wiley, 2005.

[19] F. Harris, "On the use of windows for harmonic analysis with the discrete Fourier transform," *Proc. IEEE*, vol. 66, no. 1, pp. 51–83, Jan. 1978.

[20] G. Agrawal, *Nonlinear Fiber Optics*. New York, NY, USA: Academic, 2007.

[21] S. Ghafoor and P. Petropoulos, "Effect of dispersion slope of highly nonlinear fibre on the performance of Self Phase Modulation based 2R-optical regenerator," in *Proc. 2nd Int. Conf. Comput. Technol. Develop.*, Nov. 2010, pp. 144–148.

Thibault North received the M.Sc. degree in engineering from the University of Applied Sciences and Arts, Western Switzerland in 2011. He is currently working toward the Ph.D. degree at the Photonic Systems Group, McGill University, Montréal, QC, Canada.

Martin Rochette is currently an Associate Professor with the Department of Electrical and Computer Engineering, McGill University, Montréal, QC, Canada. He has authored or coauthored more than 120 journal and conference papers on highly non-linear materials and devices, fiber laser sources, optical fiber components, and optical communication systems. His current research interests include the application of nonlinear effects for devices and laser sources with applications for biomedicine, instrumentation, and telecommunication systems.